

# Barred galaxies in the EAGLE cosmological hydrodynamical simulation

David G. Algorry<sup>1,2\*</sup>, Julio F. Navarro<sup>3,4</sup>, Mario G. Abadi<sup>1,2</sup>, Laura V. Sales<sup>5</sup>,  
Richard G. Bower<sup>6</sup>, Robert A. Crain<sup>7</sup>, Claudio Dalla Vecchia<sup>8,9</sup>, Carlos S. Frenk<sup>6</sup>,  
Matthieu Schaller<sup>6</sup>, Joop Schaye<sup>10</sup>, and Tom Theuns<sup>6</sup>.

<sup>1</sup> Instituto de Astronomía Teórica y Experimental, CONICET-UNC, Laprida 854, X5000BGR, Córdoba, Argentina

<sup>2</sup> Observatorio Astronómico de Córdoba, Universidad Nacional de Córdoba, Laprida 854, X5000BGR, Córdoba, Argentina

<sup>3</sup> Department of Physics & Astronomy, University of Victoria, Victoria, BC V8P 5C2, Canada

<sup>4</sup> Senior CIFAR Fellow

<sup>5</sup> Department of Physics and Astronomy, University of California, Riverside, CA, 92521, USA

<sup>6</sup> Institute for Computational Cosmology, Department of Physics, Durham University, South Road, Durham, DH1 3LE, UK

<sup>7</sup> Astrophysics Research Institute, Liverpool John Moores University, 146 Brownlow Hill, Liverpool L3 5RF, UK

<sup>8</sup> Instituto de Astrofísica de Canarias C/ Vía Láctea s/n 38205 La Laguna, Tenerife, Spain

<sup>9</sup> Departamento de Astrofísica, Universidad de La Laguna, Av. del Astrofísico Francisco Sánchez s/n, 38206 La Laguna, Tenerife, Spain

<sup>10</sup> Leiden Observatory, Leiden University, P.O. Box 9513, 2300 RA Leiden, the Netherlands

Accepted XXX. Received YYY; in original form ZZZ

## ABSTRACT

We examine the properties of barred disc galaxies in a  $\Lambda$ CDM cosmological hydrodynamical simulation from the EAGLE project. Our study follows the formation of 269 discs identified at  $z = 0$  in the stellar mass range  $10.6 < \log M_*/M_\odot < 11$ . These discs show a wide range of bar strengths, from unbarred discs ( $\approx 60\%$ ) to weak bars ( $\approx 20\%$ ) to strongly barred systems ( $\approx 20\%$ ). Bars in these systems develop after redshift  $\approx 1.3$ , on timescales that depend sensitively on the strength of the pattern. Strong bars develop relatively quickly (in a few Gyr,  $\sim 10$  disc rotation periods) in systems that are disc dominated, gas poor, and have declining rotation curves. Weak bars develop more slowly in systems where the disc is less gravitationally important, and are still growing at  $z = 0$ . Unbarred galaxies are comparatively gas-rich discs whose rotation speeds do not exceed the maximum circular velocity of the halos they inhabit. Bar lengths compare favourably with observations, ranging from 0.2 to 0.8 times the radius containing 90% of the stars. Bars slow down remarkably quickly as they grow, causing the inner regions of the surrounding dark halo to expand. At  $z = 0$  strong bars have corotation radii roughly ten times the bar length. Such slow bars are inconsistent with the few cases where pattern speeds have been measured or inferred observationally, a discrepancy that, if confirmed, might prove a challenge for disc galaxy formation in  $\Lambda$ CDM.

**Key words:** Galaxy: disc – Galaxy: formation – Galaxies: kinematics and dynamics – Galaxy: structure

## 1 INTRODUCTION

The stellar discs of spiral galaxies are dynamically fragile structures prone to morphological and dynamical transformation. These might be triggered by external processes, such as accretion events, mergers, or the tidal effects of satellites and neighbouring galaxies. They may also result from internal processes, which tend to be

more subtle and to operate over longer timescales but are nonetheless effective at inducing notable changes in the morphology and structure of the disc. Internal processes invariably redistribute the disc’s angular momentum, driving mass inwards while pushing angular momentum outwards.

Angular momentum redistribution requires non-axisymmetric features (Lynden-Bell & Kalnajs 1972; Tremaine & Weinberg 1984), of which bars—i.e., extended and radially-coherent  $m = 2$  perturbations to the disc’s azimuthal structure—are a particularly

\* E-mail: david@oac.unc.edu.ar

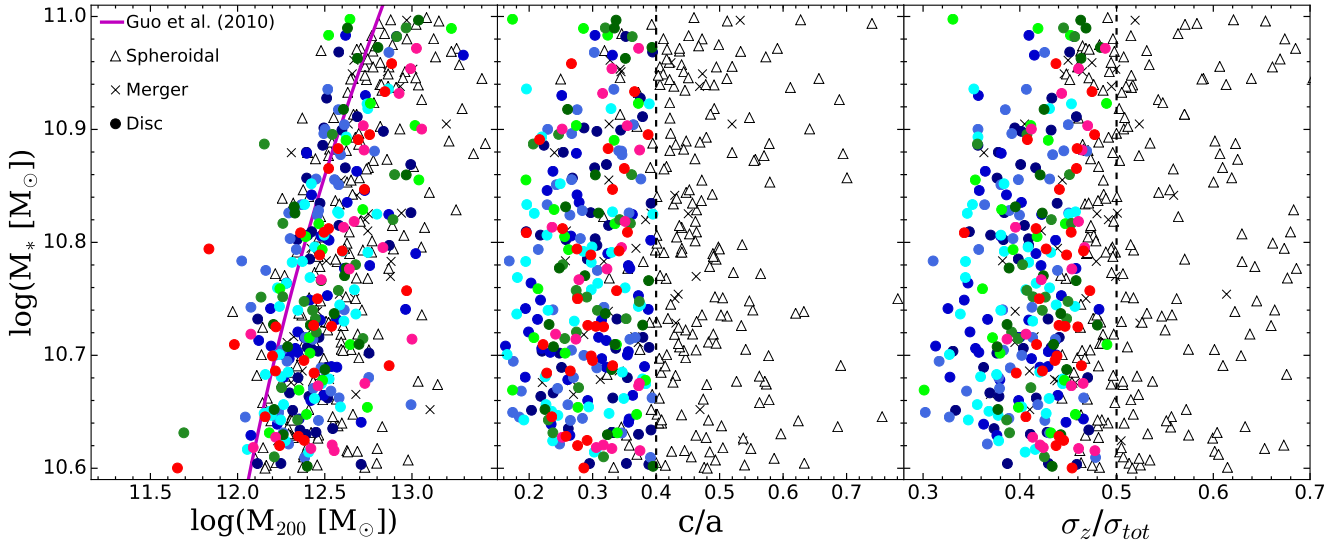


**Figure 1.** Disc galaxy sample from EAGLE used in this paper. *Left:* Galaxy stellar mass,  $M_*$ , as a function virial mass  $M_{200}$ . Solid line indicates the prediction of the abundance-matching model of Guo et al. (2010), for reference. *Middle:* Flattening parameter  $c/a$ , measured as the ratio of the eigenvalues of the principal axes of the inertia tensor of the stars. *Right:* Minor axis stellar velocity dispersion, expressed in units of the total. Vertical dashed lines indicate the conditions required to be selected as “discs” in our analysis. Discs are shown as coloured circles, spheroidal systems as open triangles, and visually identified ongoing mergers or disturbed systems as crosses. The colour scheme denotes the strength of the bar pattern (see Fig. 5).

clear example. Bars come in many different sizes and shapes; from short inner bars that affect a small fraction of stars to long bars that extend out to the confines of the disc; and from thin rectangular bars that correspond to a single, dominant  $m = 2$  mode to fat oval structures with sizable contributions from higher even Fourier modes. Taking them all together, bars are an extremely common phenomenon in disc galaxies, and are present in a large fraction of discs (e.g., Eskridge et al. 2000; Whyte et al. 2002; Marinova & Jogee 2007; Sheth et al. 2008; Gadotti 2011).

The origin of bars has long been an issue of debate. N-body discs quickly turned into bars in early simulations (Miller & Prendergast 1968; Hockney & Hohl 1969), a result that suggested a “global instability” that would affect essentially all stellar discs unless stabilized by a suitable mechanism (see Sellwood & Wilkinson 1993, for a review of early work). One such mechanism was proposed by Ostriker & Peebles (1973), who argued, in an influential paper, that cold stellar discs required the presence of a massive non-rotating dark halo in order not to go bar unstable. In this scenario, bars develop quickly in systems where the disc is dominant (perhaps triggered by accretion events or tides), whereas unbarred discs are those whose dynamics is largely dominated by the dark halo (Efstathiou et al. 1982). This idea is still widely in use and criteria for instantaneous “bar instability” are a key ingredient of semi-analytic models of galaxy formation that attempt to match the morphological mix of the observed galaxy population (see, e.g., Lacey et al. 2015, and references therein).

More recent work, however, has led to a more nuanced view, and it is now recognized that bars, weak and strong, may develop gradually in most stellar discs that are relatively massive and kinematically cold, even when the halo is important. Indeed, in some cases massive halos have even been found to promote bar formation: one clear example is that provided by Athanassoula (2002), who shows that bars may develop faster in disc-dominated systems, but they eventually become stronger in halo-dominated ones. Halos

apparently do not prevent bars, but, rather, just delay their formation (see Athanassoula 2013, for a recent review).

Once formed, bars are a conduit for the transfer angular momentum from the disc to other parts of the system. The more angular momentum a bar is able to lose, the longer and thinner (“stronger”) it can become. To grow, then, bars need material to absorb the angular momentum lost by stars that join the bar, be it other stars in the outer disc or particles in the halo that might get trapped in resonances with the bar. A massive halo can therefore aid this process by providing a sink for the angular momentum lost by stars that make up the growing bar (Athanassoula 2003).

Bars can therefore develop gradually over many orbital periods, on a timescale that depends mainly on the relative importance of disc vs halo, but likely influenced as well by the velocity dispersion of the disc (hotter discs are less prone to global distortions) and by the potential well depth of the halo (faster moving halo particles are harder to trap into resonances with the bar). The two scenarios—instantaneous bar instability vs gradual bar growth—should in principle yield different predictions for the abundance, size, and pattern speeds of bars, as well as for their evolution with redshift, but detailed predictions in a proper cosmological setting have yet to be worked out.

One corollary of gradual bar formation is that bars that grow longer/stronger should slow down (Hernquist & Weinberg 1992; Debattista & Sellwood 2000). This is because bars cannot extend beyond corotation, the radius where the angular speed of a circular orbit equals that of the bar pattern (Contopoulos 1980). Angular speeds decrease outwards, so the longer the bar grows the slower its pattern speed must become. The bar cannot grow longer than the disc, of course, but it can continue to slow down, implying that the ratio between corotation radius ( $r_{\text{corot}}$ ) and bar length ( $l_{\text{bar}}$ ) can provide interesting constraints on the relative importance of the disc and halo, as well as on the time elapsed since the onset of the bar (Debattista & Sellwood 2000). Although the measurements are challenging and often indirect, most observational estimates point

to “fast bars” where  $r_{\text{corot}} < 1.4 l_{\text{bar}}$  (see, e.g., Elmegreen et al. 1996; Corsini 2011).

Interestingly, bar slowdown might also have discernible effects on the dark matter density profile, since it is the halo that absorbs much of the disc angular momentum, especially in the case of strong bars. A number of studies have indeed suggested that the central density cusps expected in cold dark matter halos (Navarro et al. 1996, 1997) might be softened and perhaps erased<sup>1</sup> by a bar (Weinberg & Katz 2002; Holley-Bockelmann et al. 2005). This result has important consequences for models of gamma ray emission by dark matter annihilation in the direction of the Galactic centre (Schaller et al. 2016): the Milky Way is, after all, a barred galaxy (e.g., Blitz & Spergel 1991).

The discussion above suggests that the abundance of barred galaxies, together with the distribution of bar strengths, lengths, and pattern speeds, may provide interesting constraints on the mass, size, and kinematics of disc galaxies, on the time of their assembly, and on the mass and density profiles of the dark matter halos they inhabit. This is important, because, once a cosmological model has been adopted, the very same properties that govern bar growth are independently specified by other constraints, and cannot be tuned arbitrarily. Success in reproducing the properties of the barred galaxy population in a particular cosmology is thus far from assured.

In  $\Lambda$ CDM models—the current paradigm of structure formation—the relation between galaxy mass and halo mass may be derived using “abundance matching” arguments (Frenk et al. 1988; Vale & Ostriker 2006; Guo et al. 2010; Moster et al. 2013; Behroozi et al. 2013). Further, galaxy sizes are also constrained by scaling laws such as the Tully-Fisher relation (see, e.g., Ferrero et al. 2016). Do galaxies that match those constraints also result in a barred galaxy population whose statistics, bar lengths, and pattern speeds are compatible with observation?

We address this question here by examining the properties of disc galaxies in the EAGLE cosmological hydrodynamical simulation of a  $\Lambda$ CDM universe (Schaye et al. 2015; Crain et al. 2015). This paper is organized as follow. In Sec. 2 we briefly describe the numerical simulations and the galaxy sample selection. Sec. 3 presents the results of our analysis, including the frequency of bars (Sec. 3.2); bar lengths (Sec. 3.3); bar growth (Sec. 3.5); bar slowdown (Sec. 3.6); and its effects on the halo mass profile (Sec. 3.7). We summarize our main conclusions in Sec. 4.

## 2 NUMERICAL SIMULATION AND SAMPLE SELECTION

### 2.1 The EAGLE simulation

We use galaxies identified in one of the cosmological hydrodynamical simulations of the EAGLE (Evolution and Assembly of GaLaxies and their Environments) Project. This run, labelled “Ref-L100N1504” in Schaye et al. (2015), follows the evolution of  $2 \times 1504^3$  particles (baryons + dark matter) in a large cosmological box with 100 comoving Mpc on a side, adopting a flat  $\Lambda$ CDM cosmology consistent with the cosmological parameters from the Planck Collaboration (2014):  $H_0 = 67.77 \text{ km s}^{-1}$ ,  $\sigma_8 = 0.8288$ ,  $n_s = 0.9611$ ,  $\Omega_m = 0.307$ ,  $\Omega_\Lambda = 0.693$  and  $\Omega_b = 0.04825$ .

Initial conditions were generated using second order Lagrangian perturbation theory (Jenkins 2010) for gas and dark matter particles with masses equal to  $1.81 \times 10^6 M_\odot$  and  $9.70 \times 10^6 M_\odot$ , respectively. The Plummer-equivalent gravitational softening is set to 2.66 comoving kpc and capped to a maximum physical value of 0.7 kpc at  $z = 2.8$ . Full particle properties are recorded at 29 snapshots between redshift 20 and 0. In addition, a reduced set of particles properties are recorded at 405 outputs between redshift 20 and 0. For a detailed description of the simulations we refer the reader to Schaye et al. (2015).

The simulation was performed using a modified version of the GADGET3 code, a descendant of GADGET2 (Springel 2005), with a version of Smoothed Particle Hydrodynamics (SPH) technique modified to a pressure-entropy formulation of the equations of motion (Hopkins 2013; Schaller et al. 2015b). The simulation includes a prescription for radiative cooling and heating implemented following Wiersma et al. (2009a).

Star formation is treated stochastically following the pressure-dependent Kennicutt-Schmidt relation (Schaye & Dalla Vecchia 2008), with a metal-dependent density threshold (Schaye 2004). The stellar initial mass function is assumed to be that of Chabrier (2003) and the stellar mass loss is modelled (Wiersma et al. 2009b). Feedback from star formation is implemented thermally and stochastically following Dalla Vecchia & Schaye (2012). Black holes growth is modelled using a modified version of the Bondi-Hoyle accretion and can input energy to their surrounding gas through AGN feedback (Rosas-Guevara et al. 2016).

The subgrid parameters of EAGLE have been calibrated to match the galaxy stellar mass function and the average size of galaxies as a function of mass at  $z = 1$ . Earlier papers have demonstrated that EAGLE broadly reproduces a number of well known properties of the galaxy population, including their colours, metallicities, alpha-enhancement, star formation rates, gas content, and scaling laws (Furlong et al. 2015; Lagos et al. 2015; Rahmati et al. 2015; Schaller et al. 2015a; Schaye et al. 2015; Trayford et al. 2015, 2016; Bahé et al. 2016; Camps et al. 2016; Segers et al. 2016).

### 2.2 Galaxy sample

Dark matter haloes are identified at every snapshot using a friends-of-friends (FoF) algorithm with linking length equal to 0.2 times the mean interparticle separation (Davis et al. 1985). Baryonic particles are then assigned to the same FoF halo as their closest dark matter neighbour. Gravitationally bound subhaloes are then identified in each FoF halo using the SUBFIND algorithm (Springel et al. 2001; Dolag et al. 2009). We shall only consider the most massive (“central”) subhalo of each FoF grouping and neglect “satellite” galaxies in the analysis that follows.

Our sample includes systems within a narrow range of stellar mass,  $10.6 \leq \log(M_*/M_\odot) \leq 11$ , measured within a sphere of 30 kpc radius centred at the potential minimum of the halo. We shall refer to the radius containing half of all stars as  $r_{50}$  and that containing 90% of all stars as  $r_{90}$ .

We focus our analysis on individual galaxies resolved with at least 20,000 star particles and more than 100,000 dark matter particles, so as to be able to discern their morphological traits (discs, spheroids, bars) and measure their internal structure. This resolution is at the limit of what is currently achievable in simulations that aim to resolve the galaxy population in a cosmologically significant volume. Although it is by no means ideal to follow in detail the intricate internal dynamics governing the evolution of barred galaxies (many authors argue that many millions of particles per galaxy

<sup>1</sup> Others, however, have argued otherwise, so the issue is still under debate (Sellwood 2003, 2008; Dubinski et al. 2009).

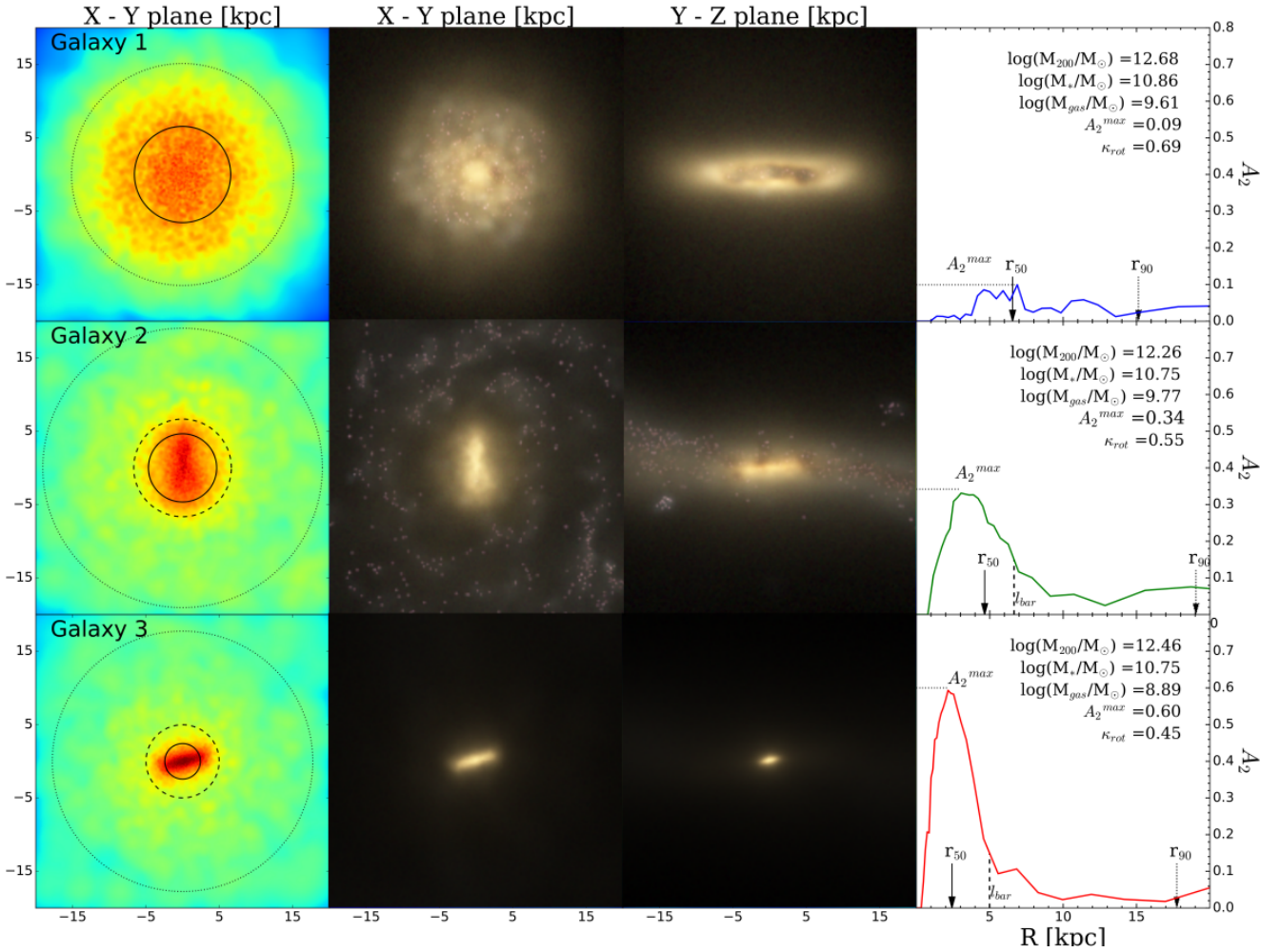


**Figure 2.** Projected stellar density maps for three examples of an unbarred galaxy (top row), a weak bar (middle row) and a strongly barred disc (bottom row). The leftmost column shows face-on views of the three galaxies. Dotted, dashed, and solid circles on the images indicate the galaxy radius,  $r_{90}$ , the bar length,  $l_{\text{bar}}$ , and the stellar half-mass radius,  $r_{50}$ . The middle and right panels show face-on and edge-on views, respectively, created with the radiative transfer code SKIRT (Baes et al. 2011). These images show the stellar light based on monochromatic SDSS  $u$ ,  $g$  and  $r$  band filters and accounting for dust extinction. The rightmost column shows the radial profile of the bar strength parameter,  $A_2(R)$ , and indicates a few characteristic radii.

are required, see, e.g., Weinberg & Katz 2007a), we believe that this is still an instructive exercise, especially because ours is one of the first studies of barred galaxies *as a population* in a proper cosmological setting. Earlier work has mainly focussed on “zoom-in” simulations of individual systems (Curir et al. 2006; Scannapieco & Athanassoula 2012; Kraljic et al. 2012; Guedes et al. 2013; Okamoto et al. 2014; Goz et al. 2015) and can therefore not address the questions we pose here.

There are 495 central galaxies that satisfy our selection criteria at  $z = 0$ . Fig. 1 shows some of the properties of this sample. As a function of stellar mass, the left panel shows the virial<sup>2</sup> mass of the system; the middle panel shows its flattening, using the axis ratio  $c/a$  of the inertia tensor principal axes; whereas the right-hand panel shows the vertical (i.e., along the axis parallel to the stars’

angular momentum) velocity dispersion,  $\sigma_z$ , in units of the total velocity dispersion of stars in the system,  $\sigma_{\text{tot}}$ .

As shown by the solid line in the left-hand panel of Fig. 1 EAGLE central galaxies in this mass range follow roughly the abundance-matching relation expected between  $M_*$  and  $M_{200}$  from the model of Guo et al. (2010). We identify discs as flattened systems kinematically cold in the vertical direction that satisfy simultaneously the following two conditions:  $c/a < 0.4$  and  $\sigma_z < 0.5 \sigma_{\text{tot}}$ . Discs are shown as coloured filled circles in Fig. 1; other galaxies are shown as either open triangles (“spheroidals”) or crosses for ongoing mergers identified through individual visual inspection. Our final sample contains 269 discs, 193 spheroidals, and 33 ongoing mergers. We shall only consider discs in the analysis that follows.

We divide the sample of discs into three categories: different hues of red for strong bars, of green for weak bars, and of blue for unbarred systems (Sec. 3.1). Note that in the right-hand panel of Fig. 1 strong bars tend to be located in discs with higher vertical velocity dispersion. This is likely the result of the three-dimensional structure of the bars and of the effect of the “buckling instability”

<sup>2</sup> Throughout this paper, virial quantities are computed within radius where the enclosed density is 200 times the critical density of the Universe and are denoted by a “200” subscript.

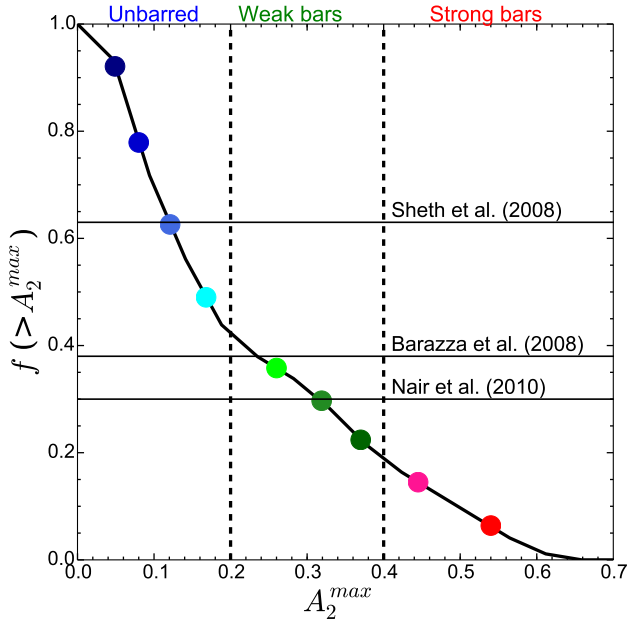


**Figure 3.** Cumulative distribution of the bar strength parameter  $A_2^{\max}$ , compared with observational estimates of the bar fraction of galaxies with comparable stellar mass. The colour scheme assigns different hues of red to strong bars ( $A_2^{\max} > 0.4$ ), of green to weak bars ( $0.2 < A_2^{\max} < 0.4$ ), and of blue to unbarred systems ( $A_2^{\max} < 0.2$ ).

(Raha et al. 1991), which tend to make discs thicker after a bar forms.

### 3 RESULTS

#### 3.1 Bars in simulated discs

We identify bars in our simulated discs by measuring the amplitude of the  $m = 0$  and  $m = 2$  Fourier modes of the azimuthal distribution of disc particles in the plane perpendicular to the angular momentum vector of stars in the galaxy. In practice, we measure

$$a_m(R) = \sum_{i=1}^{N_R} M_i \cos(m \phi_i), \quad (1)$$

and

$$b_m(R) = \sum_{i=1}^{N_R} M_i \sin(m \phi_i), \quad (2)$$

where  $N_R$  is the number of stellar particles in a given cylindrical annulus of mean radius  $R$ ,  $M_i$  is the mass of the  $i$ -th particle and  $\phi_i$  is its azimuthal angle (Athanasoula 2012).

We use the ratio

$$A_2(R) = \frac{\sqrt{a_2^2 + b_2^2}}{a_0}, \quad (3)$$

to measure the strength of the  $m = 2$  mode, and shall use its maximum value  $A_2^{\max} = \max(A_2(R))$  as a measure of the strength of the bar component.

Fig. 2 shows projected stellar density maps for three simulated galaxies with different values of  $A_2^{\max}$ . The top row shows a galaxy with  $A_2^{\max} \approx 0.1$ , where no obvious bar is present (Galaxy

1). The middle row shows a system with a clear oval structure resembling a weak bar (Galaxy 2;  $A_2^{\max} \approx 0.35$ ). Finally, the bottom row shows a strongly barred case, where  $A_2^{\max} \approx 0.6$  (Galaxy 3). We shall hereafter use the value of  $A_2^{\max}$  to classify galaxies as unbarred ( $A_2^{\max} < 0.2$ ), weakly barred ( $0.2 < A_2^{\max} < 0.4$ ), and strongly barred ( $A_2^{\max} > 0.4$ ). Although  $A_2^{\max}$  could in principle also be large for two-armed spirals, these typically peak at lower values than those we have used to define bars. We have visually checked every galaxy to make sure that our barred galaxies do not include spurious cases.

The right-hand column of Fig. 2 shows the radial profile of  $A_2$  for the three examples, and indicates a few characteristic radii:  $r_{50}$ ,  $r_{90}$ , and the bar length,  $l_{\text{bar}}$ , which we define as the radius where the  $A_2$  profile first dips below 0.15 after reaching its peak. Various circles indicate these radii on the galaxy images; note that this definition of  $l_{\text{bar}}$  (dashed circles) coincides well with the radial extent of the bar, as measured from the face-on map of the stellar distribution.

Finally, we shall use  $\phi_{\text{bar}} = 0.5 \tan^{-1}(b_2/a_2)$ , measured at the radius where  $A_2(R)$  peaks, to define the bar position angle. The time variation of this angle is used to estimate the bar pattern speed in the analysis that follows.

#### 3.2 Bar frequency

Although qualitatively there is broad consensus that bars are relatively common, quantitatively there is less agreement on the fraction of discs that are barred. This is a result of several factors, including the facts that (i) there is no standard definition of what constitutes a bar; that (ii) bar prominence depends on wavelength (stronger in the infrared; e.g., Eskridge et al. 2000), morphological type (longer in early-type spirals; e.g., Elmegreen & Elmegreen 1985), galaxy mass (decreasing with increasing mass; e.g., Nair & Abraham 2010), and redshift (less frequent at early times; e.g., Sheth et al. 2008); and that (iii) various studies differ on how to define the parent population of discs (would a galaxy be classified as barred or as a spheroid if it had no obvious disc component?).

Although these shortcomings hinder a definitive comparison of our results with observations, we contrast our findings with a few recent observational estimates in Fig. 3. This figure shows the cumulative distribution of our bar strength parameter  $A_2^{\max}$  and compares it with the bar fraction estimates of three studies that report bar fractions as a function of galaxy mass.

More specifically, Barazza et al. (2008) report a fraction of  $\approx 38\%$  for galaxies in the mass range considered in our analysis. On the other hand, Sheth et al. (2008) find, at low redshift and in the same mass range, a much higher bar fraction of  $\approx 62\%$ . Finally, Nair & Abraham (2010) report a much lower bar fraction of only about 30% in a comparable mass range. Given these disparate estimates, our finding that about 40% of EAGLE discs have bars (weak or strong) seems quite consistent with observations.

#### 3.3 Bar lengths

As discussed in Sec. 1, the length of a bar is an important parameter characterizing the evolutionary stage of the bar phenomenon. Bars are expected to grow longer with time so, if bars were triggered too early and/or their growth timescales were too short, then bar lengths, when expressed in units of the disc characteristic radii, would be too long. Such concerns have been raised by Erwin (2005), for example, who argue that there is a shortage of “short bars” in simulations.

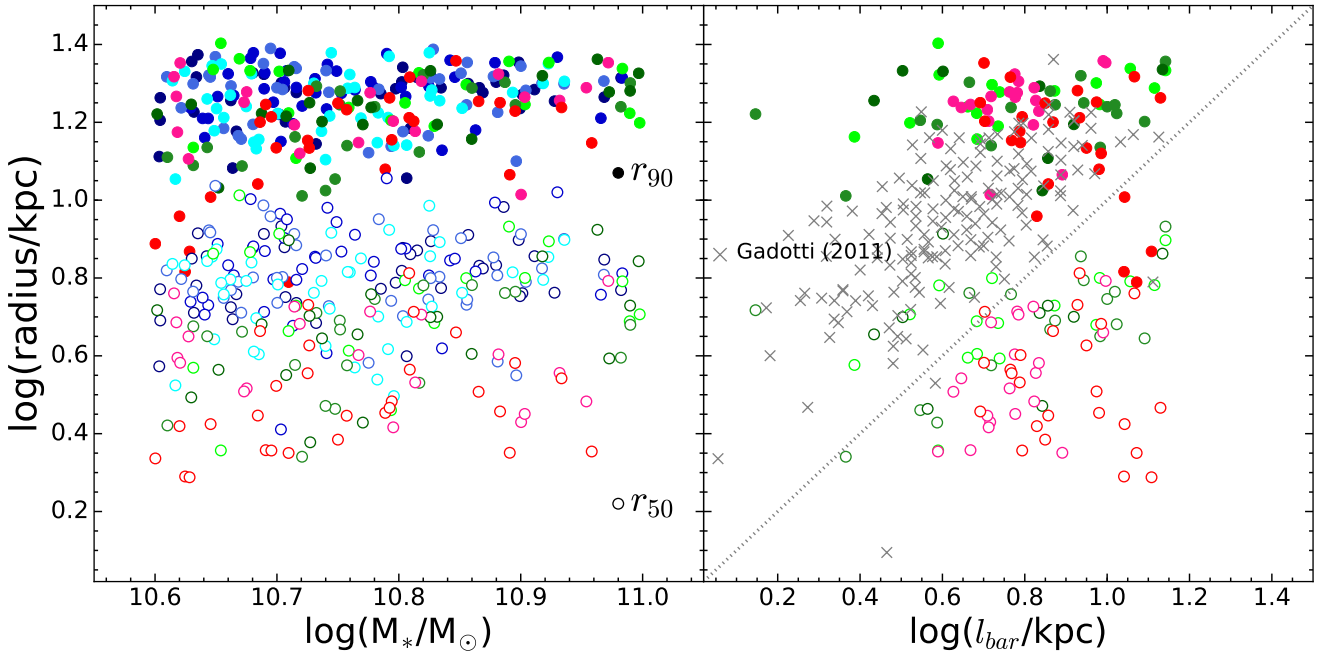


**Figure 4.** Bar lengths and disc characteristic radii. *Left:* Stellar half-mass radius and 90%-mass radius as a function of galaxy stellar mass,  $M_*$ . *Right:* Bar length compared with disc radii for galaxies with  $A_2^{\max} > 0.2$ . Colours indicate bar strength, as in Fig. 3. Grey symbols indicate  $l_{\text{bar}}$  vs  $r_{90}$  results from the SDSS observations of Gadotti (2011), for reference. Note that most of his galaxies are smaller (less massive) than those in our sample.

We examine the length of bars in Fig. 4, where the left panel shows, as a function of the galaxy stellar mass, the half-mass radius and 90%-mass radius of all EAGLE discs. The right-hand panel shows the same radii, but as a function of bar length, for all barred EAGLE galaxies ( $A_2^{\max} > 0.2$ ). Note that bar lengths tend to straddle both radii; in general  $r_{50} < l_{\text{bar}} < r_{90}$ . Relative to  $r_{90}$ , bar lengths span the whole available range: the shortest bars have  $l_{\text{bar}} \sim 0.15 r_{90}$ ; the longest reach  $l_{\text{bar}} = r_{90}$  and even exceed it in a few cases. There is certainly not a shortage of short bars in our simulations, at least as measured by  $l_{\text{bar}}/r_{90}$ .

The EAGLE predictions are in broad agreement with the results of Gadotti (2011), who show that the distribution of bar lengths in his sample of nearly 1,000 SDSS galaxies peaks at roughly  $\sim 0.6 r_{90}$ . In addition, there are few bars shorter than  $0.25 r_{90}$  or longer than  $0.85 r_{90}$ . His results for  $r_{90}$  vs  $l_{\text{bar}}$  are shown in the right-hand panel of Fig. 4 with grey crosses. Although many galaxies in the observed sample are less massive, and thus smaller than ours, it is clear that there is no obvious discrepancy between observations and simulations in the regime where they overlap in  $r_{90}$ . We conclude that bar lengths in EAGLE galaxies are well within the range allowed by observations.

### 3.4 Barred galaxy properties at $z = 0$

We now explore the relation (at  $z = 0$ ) between bar strength and the properties of the discs in which they form. Fig. 5 shows that bars are stronger in discs that are more centrally concentrated (i.e., smaller half-mass radii), that bars are relatively gas poor, and that they have formed fewer stars in the past Gyr than other discs.

Indeed, unbarred galaxies in our sample are typically forming stars at rates roughly about 40% of their past average. However, star formation rates decrease strongly with increasing bar strength, to roughly 1% of the past average for the strongest bars. A related

result is that barred discs differ strongly from unbarred ones in their star formation history. Indeed, on average, 50% (90%) of all stars in our strong bars have formed by cosmic time  $t = 3.76$  (6.15) Gyr, compared with  $t = 5.45$  (11.06) Gyr for unbarred systems.

As shown by Fig. 5, strongly-barred discs are roughly three times smaller than unbarred systems of similar stellar mass. This is an important clue that bar formation proceeds more rapidly in systems where the stellar component is more gravitationally dominant. We turn our attention to the timescale of bar growth next.

### 3.5 Bar growth

Fig. 6 shows the evolution of the bar strength parameter, averaged for galaxies binned as a function of their value of  $A_2^{\max}$  at  $z = 0$ , for the sake of clarity. This shows that bars have developed in these systems only in the past 8 Gyrs; indeed, at  $z \sim 1.3$  ( $t \sim 5$  Gyr) very few, if any, of the present day EAGLE discs in our sample had a measurable bar. Note that this statement only applies to the current sample, and should *not* be understood as implying that the bar fraction in EAGLE necessarily declines with redshift. We intend to address that topic in future work, but restrict ourselves here to the evolution of  $z = 0$  EAGLE discs within a narrow range of stellar mass, as described in Sec. 2.2.

Fig. 6 illustrates a number of interesting points: (i) bars, especially strong ones, are in general not a recurrent phenomenon; (ii) strong bars develop quickly and saturate, whereas weak bars are still growing at  $z = 0$ ; (iii) few unbarred galaxies have had bars in the past; and, finally, (iv) the timescale for bar growth is clearly a strong function of final bar strength. (We have explicitly checked that none of these conclusions are a result of the averaging procedure.) We illustrate this by the dotted line in Fig. 6, which indicates the timescale  $\tau_{\text{bar}}$  (defined as the time needed for a bar to grow from  $A_2^{\max} = 0.2$  to 0.4) as a function of final bar strength.

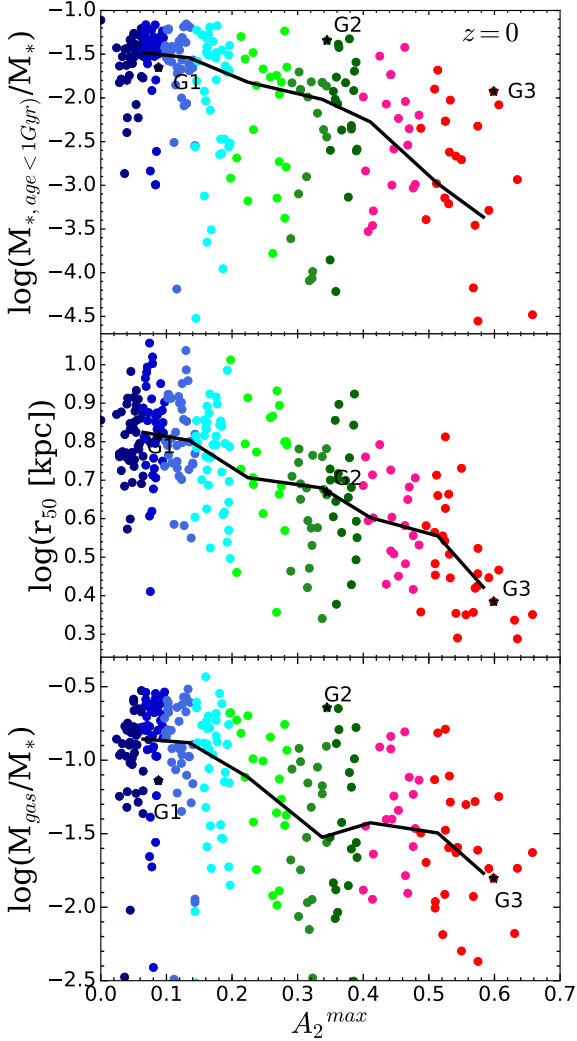


**Figure 5.** Bar strength parameter  $A_2^{\max}$  as a function of gas mass fraction (bottom), of half-mass radius (middle) and of the stellar mass form in the last Gyr at  $z = 0$  for all discs in our sample. Solid lines trace the median as a function of bar strength. G1, G2 and G3 refer to Galaxies 1, 2 and 3 in Fig. 2, respectively.

Note that even strong bars grow over several Gyr, or tens of half-mass disc rotation periods<sup>3</sup>. Weak bars take much longer to develop. We conclude that bars in EAGLE discs are best described as developing gradually over many rotation periods rather than as the result of a “global instability” that proceeds nearly instantaneously when triggered.

What sets the bar growth timescale? Or, more generally, what parameter best predicts the development of a bar? A clue may be gleaned from Fig. 5, where we showed that barred discs are on average more centrally concentrated than unbarred ones: this is in agreement with the findings of earlier work which suggested that gravitationally-dominant discs are the ones where bars will grow faster (see Sec. 1). A simple quantitative estimate is given by the ratio between the circular velocity at the half-mass radius,  $V_{50} =$

<sup>3</sup> The average disc rotation period of discs in our sample at  $r = 5$  kpc is 0.14 Gyr.

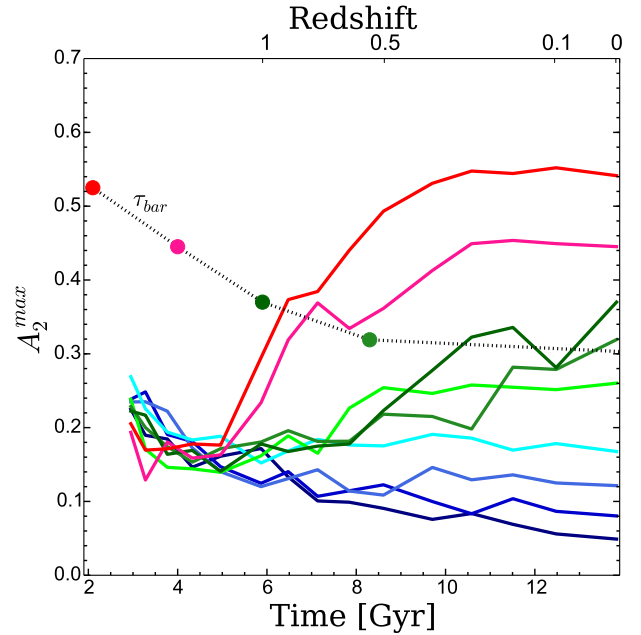


**Figure 6.** Evolution of the bar strength parameter, averaged in bins of galaxies according to their value of  $A_2^{\max}$  at  $z = 0$ . Colour scheme for the curves is as in Fig. 3. Bar growth timescales (defined arbitrarily as the time it takes to increase the bar strength from 0.2 to 0.4) are shown by the grey connected symbols. Note that this approaches the Hubble time for the weakest bars.

$V_c(r_{50})$ , and the disc contribution,  $V_{\text{disc}} = (GM_*/r_{50})^{1/2}$ ,

$$f_{\text{disc}} \equiv \frac{V_{50}}{V_{\text{disc}}}. \quad (4)$$

This type of formulation was first proposed by Efstathiou et al. (1982) and is the one usually adopted in semi-analytic models such as GALFORM (see, e.g., Cole et al. 2000; Bower et al. 2006; Lacey et al. 2015). These models typically assume that bars develop in discs with  $f_{\text{disc}} < 1.1$ , and that others remain unbarred.

The  $f_{\text{disc}}$  parameter measures the *local* importance of the disc but there is evidence to suggest that, on its own, it is insufficient to predict which galaxies will become barred. As discussed by Athanassoula & Misiriotis (2002) and Athanassoula (2003), simulations show not only that some “ $f_{\text{disc}}$ -stable” discs may become barred, but also that presumably unstable, low- $f_{\text{disc}}$  systems may be stabilized when placed within massive halos of high velocity dispersion. In other words, what matters is not just the *local* gravitational importance of the disc, but also its global importance to the whole system, including its halo.

A crude measure of the latter is provided by the ratio between the circular velocity at the half mass radius,  $V_{50}$ , and the maximum circular velocity of the surrounding halo (which typically peaks far outside the disc),

$$f_{\text{dec}} = \frac{V_{50}}{V_{\text{max,halo}}}. \quad (5)$$

With this definition, systems with  $f_{\text{dec}} < 1$  are those whose circular velocity curves rise beyond the outer confines of the disc. The smaller  $f_{\text{dec}}$  the higher the velocities of halo particles are relative to the disc, which may prevent them from coupling effectively to the bar, delaying its onset or averting it altogether. Systems with  $f_{\text{dec}} > 1$ , on the other hand, are those with “declining” rotation curves, where the disc is dominant and its rotation speed is high compared with the speed of most halo particles.

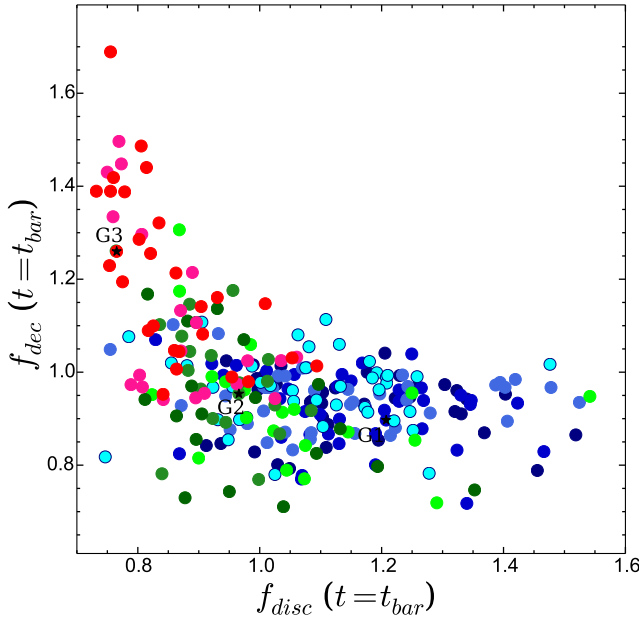


**Figure 7.** Disc gravitational importance at  $t = t_{\text{bar}}$ , defined as the time just before bars form (for weak and strong bars) or at  $z = 0.5$  for unbarred discs. The parameter  $f_{\text{disc}}$  measures the contribution of the disc to the circular velocity at the half-mass radius (Eq. 4). The parameter  $f_{\text{dec}}$  measures the global importance of the disc to the system (Eq. 5). Colour scheme is as in Fig. 3. Combining  $f_{\text{dec}}$  with  $f_{\text{disc}}$  improves predictions of which discs will develop bars. See the text for definitions and further discussion.

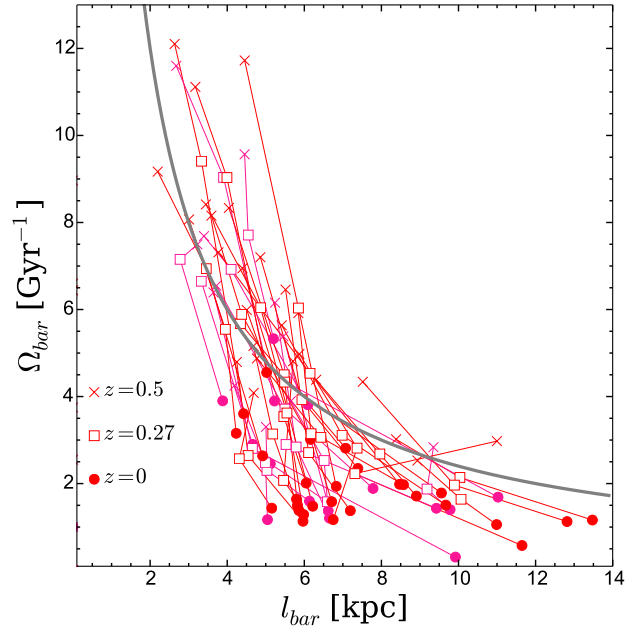
We examine this in Fig. 7, where we show  $f_{\text{disc}}$  vs  $f_{\text{dec}}$  for all galaxies in our sample, measured just *before*<sup>4</sup> the bar develops, at  $t = t_{\text{bar}}$ . This figure shows clearly that the  $f_{\text{disc}} < 1.1$  criterion does not accurately predict which galaxies will become barred: 45% of discs satisfying this criterion remain unbarred, and most such discs (73%, to be more precise) have “rising” circular velocity curves, i.e.,  $f_{\text{dec}} < 1$ .

Fig. 7 thus suggests that combining both  $f_{\text{disc}}$  and  $f_{\text{dec}}$  improves matters. For example, the combined criteria  $f_{\text{disc}} < 1$  and  $f_{\text{dec}} > 0.95$  identify 82% of strong bars. Of galaxies satisfying these criteria, only 11% remain unbarred.

Similarly, the criteria  $f_{\text{disc}} > 0.95$  and  $f_{\text{dec}} < 1$  single out 77% of all discs that remain unbarred. Of these, very few have developed strong bars (only 10) and 28 out of a total of 59 have developed weak bars. The latter are, perhaps unsurprisingly, much harder to predict on the basis of  $f_{\text{disc}}$  and  $f_{\text{dec}}$  alone, and are seen to span nearly the full range of allowed values in Fig. 7.

We conclude that, in order to develop strong bars, discs must be locally and globally dominant; in other words, they must contribute a large fraction of the inner mass budget to systems where the disc circular speed exceeds that of its halo. On the other hand, galaxies that remain unbarred are predominantly those where the disc is less important, not only within their half-mass radii but also in relation to their surrounding halos.

<sup>4</sup> In practice, we choose  $t_{\text{bar}}$  as the time when  $A_2^{\text{max}}$  first exceeds 0.2. We set  $t_{\text{bar}} = 8.6$  Gyr ( $z = 0.5$ ) for unbarred systems.



**Figure 8.** Pattern speed vs bar length for strong bars. This shows clearly that bars slow down as they grow. At early times this follows roughly the  $l_{\text{bar}} \propto \Omega_{\text{bar}}^{-1}$  scaling expected for corotation radii in discs with flat rotation curves (grey dotted curve). At late times the pattern speed slows down with little further increase in bar length, pushing corotation well beyond the edge of the bar.

### 3.6 Bar slowdown

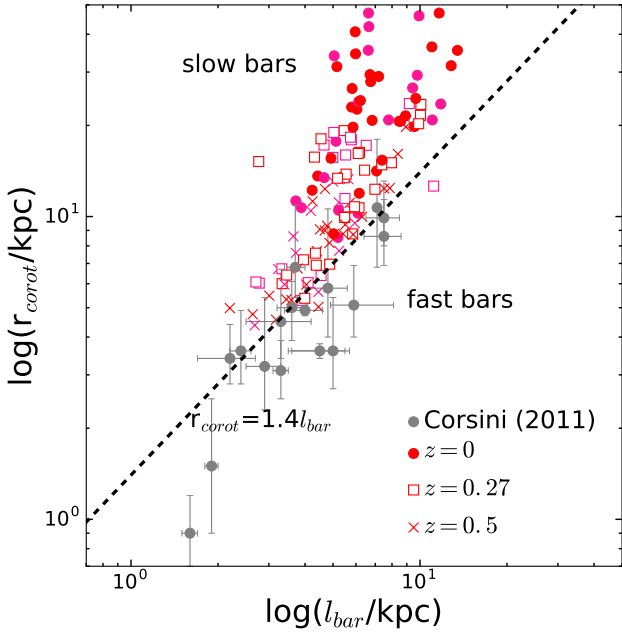
As discussed in Sec. 1, we expect bars that grow gradually to slow down as they become stronger. This is indeed the case in our simulations, as shown in Fig. 8. This figure shows the decline in the bar pattern speed,  $\Omega_{\text{bar}}$ , since  $z = 0.5$  as a function of bar length. We only show this for the “strong” bars in our sample because of difficulties estimating the pattern speed of weak bars accurately.

Fig. 8 shows that  $\Omega_{\text{bar}}$  has decreased on average by a factor of 3 over the past 5 Gyrs. In the same time interval bar lengths have increased by a factor of 1.7 on average. Indeed, the slowdown seems to roughly satisfy the  $l_{\text{bar}} \times \Omega_{\text{bar}} = \text{constant}$  relation (grey dotted line) expected for bar lengths that increase in proportion to the corotation radius in a galaxy with a flat circular velocity profile.

At late times, the slowdown proceeds in most galaxies without the corresponding increase in bar length, so that bar lengths become smaller than their corotation radii at  $z = 0$ . We examine this in more detail in Fig. 9, where we show  $r_{\text{corot}}$  vs  $l_{\text{bar}}$  for all strongly barred galaxies (as identified at  $z = 0$ ) at three different redshifts ( $z = 0.5$ ,  $z = 0.27$ , and  $z = 0$ ) and compare them with the compilation of Corsini (2011), which only includes galaxies in the local universe.

Bars below the dotted line that delineates  $r_{\text{corot}} = 1.4 l_{\text{bar}}$  are usually referred to as “fast bars”, a characterization that describes well the few galaxies for which pattern speeds have been reliably measured observationally. Note that EAGLE strong bars, although relatively fast at early times according to this characterization, have clearly become slow<sup>5</sup> by  $z = 0$  confidently.

<sup>5</sup> The few weak bars we were able to measure reliable pattern speeds for at  $z = 0$  are slightly faster, but still not as fast as observed. We do not include them in Fig. 9 because we were unable to measure pattern speeds for all of them.



**Figure 9.** Corotation radius vs bar length for *strong* bars in our sample, at three different times:  $z = 0.5$  (triangles),  $z = 0.27$  (squares), and  $z = 0$  (circles). Grey symbols with error bars are observational data from the compilation of Corsini (2011). “Fast bars” are those below the dotted line delineating  $r_{\text{corot}} = 1.4 l_{\text{bar}}$ . Most strong bars in our simulation are “slow” at  $z = 0$ , in contrast with observational estimates.

This result is reminiscent of the arguments of Debattista & Sellwood (2000), who argued that “fast bars” presented a challenge to  $\Lambda$ CDM models. In their argument, dynamical friction in halos as centrally concentrated as those expected in  $\Lambda$ CDM would quickly slow down a bar and push its corotation radius well beyond the edge of the bar, just as seen at  $z = 0$  in Fig. 9.

The Debattista & Sellwood (2000) observation ignited a spirited debate about the true slowdown rate of bars in N-body simulations that is, as far as we can tell, still unresolved (see, e.g., Sellwood 2006; Weinberg & Katz 2007a,b; Sellwood 2008, and references therein). The disagreement centres on the role of dynamical friction vs resonances, and on the minimum numerical resolution required to properly follow the bar slowdown. In particular, Weinberg & Katz (2007a) argue that several *millions* of particles would be needed to capture the resonant coupling that slows down the bar, and warn that slowdown timescales may be severely underestimated in simulations with limited numbers of particles.

The numerical resolution of our simulations is admittedly poor by comparison, so it is unclear whether our results may help to resolve this disagreement. We therefore just note that strong bars slow down very rapidly in our simulations, creating a population of “slow bars” that, apparently, have no obvious observational counterparts. If confirmed by simulations with improved numerical resolution, this may very well present a challenge to models of barred galaxy formation in a  $\Lambda$ CDM universe. Resolving this issue, however, may require much higher resolution simulations than achievable today for cosmologically significant volumes.

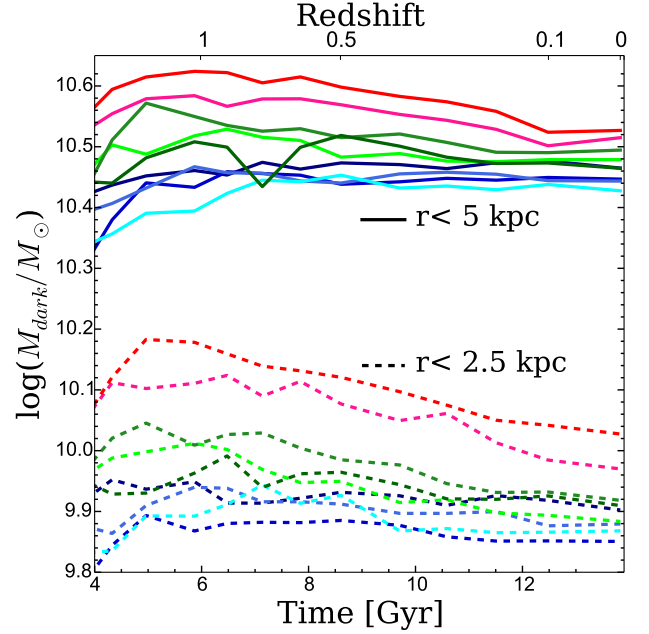


**Figure 10.** Evolution of the dark matter mass enclosed within two fixed physical radii,  $r = 5$  kpc and  $r = 2.5$  kpc, averaged for galaxies binned as a function of their bar strength at  $z = 0$  (i.e., as in Fig. 6). Bar slowdown clearly reduces the central density of dark matter within the region of the bar. By contrast, the central dark matter densities of unbarred galaxies remain unchanged during the past 5-6 Gyr.

### 3.7 Halo evolution

The dramatic bar slowdown discussed in the previous section suggests that the bar interacts strongly with the dark matter halo. This interaction leads to substantial exchange of energy and angular momentum, leading to substantial expansion of the inner regions of the halo. We show this in Fig. 10, where we plot, for various values of the bar strength, the evolution of the enclosed dark matter mass within two different radii,  $r = 2.5$  and 5 kpc. It is clear from this figure that the slowdown of the bar induces significant expansion of the inner dark matter mass profile.

Interestingly, even weak bars are able to lower the central density of dark matter significantly, implying that non-axisymmetric features in disc galaxies might be an important driver of the transformation of the inner mass profiles of their dark matter halos. By contrast, the inner regions of halos of disc galaxies that do not develop a bar evolve little over the past  $\sim 5$  Gyr or so.

Finally, Fig. 10 shows that, despite the bar-induced expansion of the inner halo, barred galaxies at  $z = 0$  still have more dark matter in their inner regions than their unbarred counterparts of similar stellar and virial mass. This is mainly because barred galaxies occur predominantly in dense, dominant discs that have substantially contracted the dark matter profile before the bar forms.

Indeed, galaxies that will become strong bars have, at  $z \sim 0.5$ , roughly twice as much dark matter within 2.5 kpc from the centre as galaxies that remain unbarred. Although the difference narrows as the bar slows down, it still remains at  $z = 0$ . This implies that the bar-induced halo expansion might not actually create a constant density “core” in a cuspy dark halo; the inner cusps of halos of would-be bars are so steep because of contraction that even after expanding they may remain cuspy. Although qualitatively our argument seems robust we are unable to examine it quantitatively

because of limited numerical resolution: the average [Power et al. \(2003\)](#) convergence radius of our systems, for example, is of order  $\sim 5$  kpc. Clarifying whether bars carve “cores” out of cusps or not will need to await simulations with much higher numerical resolution.

#### 4 SUMMARY AND CONCLUSIONS

We have used a  $\Lambda$ CDM cosmological hydrodynamical simulation from the EAGLE project to study the formation of barred galaxies. The simulation evolves a box 100 Mpc on a side with  $2 \times 1504^3$  particles, half of which are baryonic and half dark matter. Our study focusses on a narrow range of stellar mass,  $10.6 < \log M_*/M_\odot < 11$ , which are resolved with at least 22,000 star particles. Of the 495 galaxies in that mass range identified at  $z = 0$  we select a sample of 269 “discs”, defined as flattened systems with minor-to-major axis ratio  $c/a < 0.4$  and relatively low vertical velocity dispersion  $\sigma_z/\sigma_{\text{tot}} < 0.5$ .

We identify barred galaxies by measuring the amplitude of the normalized  $m = 2$  Fourier mode of the azimuthal surface density profile as a function of cylindrical radius, and choose as a measure of bar strength the peak amplitude,  $A_2^{\text{max}}$ . We consider “barred” all discs with  $A_2^{\text{max}} > 0.2$ . We follow the evolution of all these galaxies in order to estimate bar growth timescales, to identify which parameters predict the development of bars best, and to measure the evolution of bar strength, length, and pattern speed.

Our main conclusions may be summarized as follows.

- About 40% of EAGLE discs in our sample are barred, 20% of them strong bars ( $A_2^{\text{max}} > 0.4$ ) and another 20% weak bars ( $0.2 < A_2^{\text{max}} < 0.4$ ). This bar frequency seems in reasonable agreement with observational estimates from [Sheth et al. \(2008\)](#); [Barazza et al. \(2008\)](#); [Nair & Abraham \(2010\)](#).

- Bars in our simulated discs span a wide range in terms of length. They typically extend beyond the stellar half-mass radius but rarely exceed the radius containing 90% of the stellar mass, in good agreement with observational estimates. In terms of each of those radii, the median bar length and interquartile range is given by  $l_{\text{bar}}/r_{50} = 1.53_{-0.41}^{+0.42}$  and  $l_{\text{bar}}/r_{90} = 0.35_{-0.10}^{+0.18}$ .

- At  $z = 0$ , bar strength correlates strongly with stellar half-mass radius (stronger bars form in smaller discs), hinting that, as expected from earlier work, bars develop preferentially in systems where the disc is gravitationally important. We also find that stronger bars develop in systems that are less gas-rich, and that have formed the bulk of their stars earlier than unbarred discs.

- Strong bars in our sample develop relatively quickly before saturating over a few Gyrs. Weak bars are still growing in strength at  $z = 0$ , and take much longer to develop, with characteristic timescales approaching or even exceeding a Hubble time. Even our strongest, fastest growing bars take roughly 4-5 Gyr ( a few dozen disc rotations) to form fully.

- The gravitational importance of the disc at its half-mass radius may be used to predict which galaxies will develop bars, but its predictive power may be enhanced by considering the overall importance of the disc in the system as a whole. Strong bars form in discs where baryons dominate and whose rotation speeds exceed the maximum circular velocity of the halo. Unbarred galaxies are discs where baryons are less important and whose rotation curves tend to rise in the outskirts.

- Strong bars slow down quickly as they grow and, at  $z = 0$  are in the “slow bar” regime,  $r_{\text{corot}}/l_{\text{bar}} > 1.4$ . This is in contrast with

the few bars whose pattern speeds have been inferred observationally, all of which are “fast”. This discrepancy may either imply that bar slowdown rates are artificially high in simulations at EAGLE resolution (e.g., [Weinberg & Katz 2007a](#)), or, as argued in earlier work, that producing long-lasting “fast bars” is a real challenge for  $\Lambda$ CDM (e.g., [Debattista & Sellwood 2000](#)).

- The bar slowdown induces an expansion of the inner regions of the dark matter halo, as they capture the angular momentum of the forming bar. However, bars form in massive dense discs with heavily contracted halos, so despite the bar-induced expansion barred galaxy halos are still more centrally concentrated than unbarred galaxies of similar stellar mass. Our numerical resolution is not enough to let us ascertain whether this expansion may lead to the formation of constant density “cores” in barred galaxy halos.

Our overall conclusion is that current  $\Lambda$ CDM cosmological hydrodynamical simulations of cosmologically significant volumes such as EAGLE yield a population of simulated discs with bar fractions, lengths, and evolution that are in broad agreement with observational constraints. They also confirm earlier suggestions that “slow bars” might pose a severe challenge to this scenario. Although bars form in the manner and frequency expected, they slow down too fast through interaction with the dark halo. Unless the Universe has a population of slow bars that has yet to be recognized, or the bar slowdown we measure is artificially enhanced by limited numerical resolution, accounting for the presence of “fast bars” in strongly-barred discs is a clear goal for the next generation of  $\Lambda$ CDM simulations of galaxy formation.

#### ACKNOWLEDGEMENT

DA, MGA, JFN, LVS acknowledge financial support from grant PICT-1137/2012 from the Agencia Nacional de Promoción Científica y Tecnológica, Argentina. MGA acknowledges financial support of grant 203/14 of the SECYTUNC, Argentina. We are grateful to Alejandro Benítez-Llambay for the use of his PySPHViewer software. The research was supported in part by the European Research Council under the European Union’s Seventh Framework Programme (FP7/2007-2013) / ERC Grant agreement 278594-GasAroundGalaxies, 267291-COSMIWAY, by the Interuniversity Attraction Poles Programme initiated by the Belgian Science Policy Office (AP P7/08 CHARM) and by the Netherlands Organisation for Scientific Research (NWO), through VICI grant 639.043.409. This work used the DiRAC Data Centric system at Durham University, operated by the Institute for Computational Cosmology on behalf of the STFC DiRAC HPC Facility ([www.dirac.ac.uk](http://www.dirac.ac.uk)). This equipment was funded by BIS National E-infrastructure capital grant ST/K00042X/1, STFC capital grants ST/H008519/1 and ST/K00087X/1, STFC DiRAC Operations grant ST/K003267/1 and Durham University. DiRAC is part of the National E-Infrastructure. RAC is a Royal Society University Research Fellow. CDV acknowledges financial support from the Spanish Ministry of Economy and Competitiveness (MINECO) under the 2015 Severo Ochoa Program SEV-2015-0548 and grant AYA2014-58308.

#### REFERENCES

- Athanassoula E., 2002, [ApJ](#), **569**, L83  
 Athanassoula E., 2003, [MNRAS](#), **341**, 1179  
 Athanassoula E., 2012, [MNRAS](#), **426**, L46

- Athanassoula E., 2013, Bars and secular evolution in disk galaxies: Theoretical input. p. 305
- Athanassoula E., Misiriotis A., 2002, *MNRAS*, **330**, 35
- Baes M., Dejonghe H., Davies J., 2011, SKIRT: Stellar Kinematics Including Radiative Transfer, Astrophysics Source Code Library (ascl:1109.003)
- Bahé Y. M., et al., 2016, *MNRAS*, **456**, 1115
- Barazza F. D., Jogee S., Marinova I., 2008, *ApJ*, **675**, 1194
- Behroozi P. S., Marchesini D., Wechsler R. H., Muzzin A., Papovich C., Stefanon M., 2013, *ApJ*, **777**, L10
- Blitz L., Spergel D. N., 1991, *ApJ*, **379**, 631
- Bower R. G., Benson A. J., Malbon R., Helly J. C., Frenk C. S., Baugh C. M., Cole S., Lacey C. G., 2006, *MNRAS*, p. 659
- Camps P., Trayford J. W., Baes M., Theuns T., Schaller M., Schaye J., 2016, *MNRAS*, **462**, 1057
- Chabrier G., 2003, *ApJ*, **586**, L133
- Cole S., Lacey C. G., Baugh C. M., Frenk C. S., 2000, *MNRAS*, **319**, 168
- Contopoulos G., 1980, *A&A*, **81**, 198
- Corsini E. M., 2011, Memorie della Societa Astronomica Italiana Supplementi, **18**, 23
- Crain R. A., et al., 2015, *MNRAS*, **450**, 1937
- Curir A., Mazzei P., Murante G., 2006, *A&A*, **447**, 453
- Dalla Vecchia C., Schaye J., 2012, *MNRAS*, **426**, 140
- Davis M., Efstathiou G., Frenk C. S., White S. D. M., 1985, *ApJ*, **292**, 371
- Debbastista V. P., Sellwood J. A., 2000, *ApJ*, **543**, 704
- Dolag K., Borgani S., Murante G., Springel V., 2009, *MNRAS*, **399**, 497
- Dubinski J., Berentzen I., Shlosman I., 2009, *ApJ*, **697**, 293
- Efstathiou G., Lake G., Negroponte J., 1982, *MNRAS*, **199**, 1069
- Elmegreen B. G., Elmegreen D. M., 1985, *ApJ*, **288**, 438
- Elmegreen B. G., Elmegreen D. M., Chromey F. R., Hasselbacher D. A., Bissell B. A., 1996, *AJ*, **111**, 2233
- Erwin P., 2005, *MNRAS*, **364**, 283
- Eskridge P. B., et al., 2000, *AJ*, **119**, 536
- Ferrero I., et al., 2016, preprint, (arXiv:1607.03100)
- Frenk C. S., White S. D. M., Davis M., Efstathiou G., 1988, *ApJ*, **327**, 507
- Furlong M., et al., 2015, *MNRAS*, **450**, 4486
- Gadotti D. A., 2011, *MNRAS*, **415**, 3308
- Goz D., Monaco P., Murante G., Curir A., 2015, *MNRAS*, **447**, 1774
- Guedes J., Mayer L., Carollo M., Madau P., 2013, *ApJ*, **772**, 36
- Guo Q., White S., Li C., Boylan-Kolchin M., 2010, *MNRAS*, pp 367–376
- Hernquist L., Weinberg M. D., 1992, *ApJ*, **400**, 80
- Hockney R. W., Hohl F., 1969, *AJ*, **74**, 1102
- Holley-Bockelmann K., Weinberg M., Katz N., 2005, *MNRAS*, **363**, 991
- Hopkins P. F., 2013, *MNRAS*, **428**, 2840
- Jenkins A., 2010, *MNRAS*, **403**, 1859
- Kraljic K., Bournaud F., Martig M., 2012, *ApJ*, **757**, 60
- Lacey C. G., et al., 2015, preprint, (arXiv:1509.08473)
- Lagos C. d. P., et al., 2015, *MNRAS*, **452**, 3815
- Lynden-Bell D., Kalnajs A. J., 1972, *MNRAS*, **157**, 1
- Marinova I., Jogee S., 2007, *ApJ*, **659**, 1176
- Miller R. H., Prendergast K. H., 1968, *ApJ*, **151**, 699
- Moster B. P., Naab T., White S. D. M., 2013, *MNRAS*, **428**, 3121
- Nair P. B., Abraham R. G., 2010, *ApJ*, **714**, L260
- Navarro J. F., Frenk C. S., White S. D. M., 1996, *ApJ*, **462**, 563
- Navarro J. F., Frenk C. S., White S. D. M., 1997, *ApJ*, **490**, 493
- Okamoto T., Isoe M., Habe A., 2014, preprint, (arXiv:1410.0442)
- Ostriker J. P., Peebles P. J. E., 1973, *ApJ*, **186**, 467
- Plank Collaboration 2014, preprint, (arXiv:1409.2495)
- Power C., Navarro J. F., Jenkins A., Frenk C. S., White S. D. M., Springel V., Stadel J., Quinn T., 2003, *MNRAS*, **338**, 14
- Raha N., Sellwood J. A., James R. A., Kahn F. D., 1991, *Nature*, **352**, 411
- Rahmati A., Schaye J., Bower R. G., Crain R. A., Furlong M., Schaller M., Theuns T., 2015, *MNRAS*, **452**, 2034
- Rosas-Guevara Y., Bower R. G., Schaye J., McAlpine S., Dalla Vecchia C., Frenk C. S., Schaller M., Theuns T., 2016, *MNRAS*, **462**, 190
- Scannapieco C., Athanassoula E., 2012, *MNRAS*, **425**, L10
- Schaller M., et al., 2015a, *MNRAS*, **451**, 1247
- Schaller M., Dalla Vecchia C., Schaye J., Bower R. G., Theuns T., Crain R. A., Furlong M., McCarthy I. G., 2015b, *MNRAS*, **454**, 2277
- Schaller M., et al., 2016, *MNRAS*, **455**, 4442
- Schaye J., 2004, *ApJ*, **609**, 667
- Schaye J., Dalla Vecchia C., 2008, *MNRAS*, **383**, 1210
- Schaye J., et al., 2015, *MNRAS*, **446**, 521
- Segers M. C., Schaye J., Bower R. G., Crain R. A., Schaller M., Theuns T., 2016, *MNRAS*, **461**, L102
- Sellwood J. A., 2003, *ApJ*, **587**, 638
- Sellwood J. A., 2006, *ApJ*, **637**, 567
- Sellwood J. A., 2008, *ApJ*, **679**, 379
- Sellwood J. A., Wilkinson A., 1993, *Reports on Progress in Physics*, **56**, 173
- Sheth K., et al., 2008, *ApJ*, **675**, 1141
- Springel V., 2005, *MNRAS*, **364**, 1105
- Springel V., Yoshida N., White S. D. M., 2001, *New Astronomy*, **6**, 79
- Trayford J. W., et al., 2015, *MNRAS*, **452**, 2879
- Trayford J. W., Theuns T., Bower R. G., Crain R. A., Lagos C. d. P., Schaller M., Schaye J., 2016, *MNRAS*, **460**, 3925
- Tremaine S., Weinberg M. D., 1984, *ApJ*, **282**, L5
- Vale A., Ostriker J. P., 2006, *MNRAS*, **371**, 1173
- Weinberg M. D., Katz N., 2002, *ApJ*, **580**, 627
- Weinberg M. D., Katz N., 2007a, *MNRAS*, **375**, 425
- Weinberg M. D., Katz N., 2007b, *MNRAS*, **375**, 460
- Whyte L. F., Abraham R. G., Merrifield M. R., Eskridge P. B., Frogel J. A., Pogge R. W., 2002, *MNRAS*, **336**, 1281
- Wiersma R. P. C., Schaye J., Smith B. D., 2009a, *MNRAS*, **393**, 99
- Wiersma R. P. C., Schaye J., Smith B. D., 2009b, *MNRAS*, **393**, 99

This paper has been typeset from a  $\text{\LaTeX}$  file prepared by the author.